Computer Fraud and Security
ISSN (online): 1873-7056

Research on the Safety and Stability of Scraper Conveyor Drive Based on Radial Basis Function Neural Network

Da Lv[1], Chao ZHANG[2,*], Wentao ZHAO[3], Yongzhi PANG[4], Hongbo FEI[5]

[1]School of Mechanical Engineering, Inner Mongolia University of Science and Technology, Baotou, Inner Mongolia,014030, China；

[2]Baotou Vocational and Technical College, Baotou, Inner Mongolia,014030, China

**Corresponding author*

Abstract:

In order to finally achieve the purpose of online detection of scraper conveyor jam and chain breakage fault, this paper proposes a method to determine the occurrence of scraper conveyor jam and chain breakage fault by identifying the sudden change characteristics of drive motor current. In this paper, radial basis function neural network is used as the basis for the kernel algorithm calculation of the scraper conveyor drive current characteristic recognition model, and the expansion principle and data fusion method are used to complete the diagnosis and fault tolerance control of the speed sensor, and the diagnosis and fault tolerance of the current sensor are realized by the expansion observer compensation state formula. To verify the feasibility of the method, the current data simulation of the scraper conveyor operation process is combined with the field provided. The simulation results show that the control strategy proposed in this paper can achieve power down diagnosis and fault-tolerant control of speed and current sensors, which is of practical significance for the stable operation of the scraper conveyor.

Keywords: radial basis function neural network; scraper conveyor; drive current; characteristics

1 INTRODUCTION

The space of coal mine comprehensive mining working face is narrow but the production volume is high, and the equipment is mostly installed and operated under harsh environmental conditions, so the replacement of equipment parts and the handling of accidents can be quite difficult. Reliable operation of machinery and equipment is the premise of normal production of comprehensive mining working face. As a typical equipment of scraper conveyor, the working environment is harsh, heavy load is frequently started, and the electric energy loss is large, which seriously affects the operation reliability of the whole comprehensive mining working face and wastes a lot of electric energy at the same time.

For the coordinated control of motor power of multi-scraper conveyor of coal mine conveying equipment, foreign scholars have carried out relevant research earlier. Literature [1] has conducted in-depth analysis and research on the load balance of the scraper drive system, and pointed out that it is necessary to realize the coordinated power control of the drive system; Document [2] points out that in the process of coal mining, the load of the scraper is disorderly and unpredictable, and the real-time change of the load affects the power of the scraper conveyor motor of the drive system, and adopts the method of adjusting the power supply voltage frequency of the scraper conveyor motor to control the operating parameters of the scraper, and develops a control algorithm based on the rule description, By adjusting the frequency, the two drive scraper conveyor motors at the head and tail of the machine can operate in coordination to prevent the overload operation of a single scraper conveyor motor. This algorithm is conducive to reducing the friction loss and power down frequency of the scraper, and improving the operation of the scraper; In reference [3], aiming at the dynamic phenomenon of uneven load distribution on different drives observed in practical applications, the factors affecting load distribution were studied and analyzed through the establishment of a physical model of scraper conveyor and a large number of computer simulation experiments, such as the slip rate of scraper conveyor motor, the change of power supply voltage drop and frequency of scraper conveyor motor, and the difference of transmission gear ratio.

Literature [4] constructs the finite element dynamic simulation model of the scraper machine based on AMESim software, compares the influence of different starting modes on the tension of the scraper chain of the scraper machine and the load coordination of the motor of the scraper conveyor under heavy load conditions, and

verifies the necessity of using the motor sequence of the two scraper conveyors at the head and tail of the scraper machine to start and select the appropriate starting time difference; Literature [5] derives from the simplified chain drive physical model that the rated speed and synchronous speed of the motor of the scraper conveyor affect the power distribution of the motor of the scraper conveyor at the head and tail of the scraper conveyor. At the same time, by means of field investigation and theoretical analysis, it is pointed out that the starting mode of the motor of the scraper conveyor at the tail running first and the appropriate starting time difference between the two scraper conveyor motors can help to improve the power imbalance; Literature [6] uses the controllable start device CST controlled by fuzzy PID to realize the soft start of heavy scraper. Its CST hydraulic servo mechanism is modeled by the AMESim platform, and the fuzzy PID regulator is completed by MATLAB/Simulink. In the process of studying the power coordinated control of CST system, the influence of the load size and distribution of scraper and the starting time difference between the head and tail scraper conveyor motors on the power uncoordinated phenomenon is analyzed; Document [7] has made and calculated the combined characteristic curve and equation of the scraper conveyor motor and hydraulic coupler. On the premise of considering the effect of the scraper conveyor motor's own characteristics and the chain pitch change on the power of the head and tail scraper conveyor motor, the influence of rigid connection and hydraulic coupler connection on the power distribution is calculated and analyzed respectively, It is pointed out that the use of hydraulic coupler is helpful to improve the power balance of the scraper conveyor motor at the head and tail of the scraper machine; Literature [8] studies the load characteristics of the scraper conveyor. On the premise that the frequency converter drives the scraper conveyor motor, the master-slave control mode of the torque driven double scraper conveyor motor is adopted to achieve the speed coordination and torque balance of the drive system head and tail scraper conveyor motor, and then the fuzzy control rules are used to adjust the speed of the scraper conveyor motor in real time to achieve the goal of the scraper unit load balance; Literature [9] uses the electrical parameter acquisition module to extract the current data, and collects the dynamic tension value of the scraper when it passes through the sprocket through the strain gauge. The current value is input to the fuzzy PID regulator through comparison and calculation to complete the continuous adjustment of the motor speed of the tail scraper conveyor, thus compensating the output torque of the motor of the other side scraper conveyor, and making the tension difference between the front and rear sprocket of the scraper closer, The intelligent coordinated control of the motor power of the scraper conveyor is realized; Through the derivation of the mathematical model of the scraper dynamics and the construction of the simulation model, the paper [10] analyzed and concluded that the factors affecting the power of the scraper conveyor motor are the mechanical characteristics of the scraper conveyor motor, the load change, the structural parameter change of the sprocket chain, etc., and adjusted the output speed of the scraper conveyor motor according to the load torque ratio to achieve the coordinated control of power; In reference [11], aiming at the power imbalance of the three-drive scraper conveyor system, the real-time load is determined according to the torque current of the scraper conveyor motor, and then the output torque is adjusted by changing the speed of the head and tail scraper conveyor motor through the frequency converter with the direct torque control function. A simulation model is established based on the AMEsim platform, and experiments are carried out under the conditions of load stability and load fluctuation respectively according to the above scheme, The results show that the head equivalent scraper conveyor motor and the tail scraper conveyor motor both reach the rated power distribution ratio, which proves the correctness and rationality of the established scheme. The master-slave regulation method is also adopted for the dual-drive scraper system using MATLAB/Simulink software tool, that is, the overall loop is speed closed-loop vector regulation, and the corresponding torque is calculated by PI regulator, The torque of the slave machine is calculated based on the given torque distribution ratio, and then the master and slave circuits respectively complete their respective torque closed-loop regulation to achieve power coordinated control. Based on the sliding mode variable structure control principle, a motor flux and output torque regulator of the scraper conveyor is implemented, which is used in the direct torque control system of the scraper conveyor motor of the double-drive scraper machine to complete accurate torque signal tracking, With the help of modeling analysis, the controller can realize the purpose of fast and accurate tracking of the given torque distribution of the scraper conveyor motor at the head and tail of the scraper conveyor; Document [12] proposes the power coordination control scheme of the scraper drive system based on the magnetic coupling soft start device, uses MATLAB/Simulink to build the simulation model of the control system, adjusts the size of the magnetic coupling air gap according to the load change reflected by the current value of the scraper conveyor

motor, so as to increase or decrease the torque given by it, and then adjusts the output power of the scraper conveyor motor to achieve proportional output.

Literature [13] has studied the load non-uniformity of the drive device of the scraper conveyor, and considered that the drive device must have a certain power balance. Literature [14] studied the nonlinear vibration characteristics of the drive device of the scraper conveyor, and put forward suggestions on reducing vibration and improving the reliability of the drive device. Literature [15] conducted relevant experimental research on the starting characteristics of the hydraulic coupling of the scraper conveyor, and obtained data on the dynamic load of the transmission device and the voltage drop of the motor power supply, which proved that the hydraulic coupling has better performance than the elastic coupling. At the same time, Dolipski. M studies the starting dynamics characteristics of TN plate conveyor under the hydraulic coupling drive system. Literature [16] analyzes the dynamic performance of the scraper conveyor under startup, abnormal load and other working conditions in view of the hydraulic coupling and controllable slip CST drive used on the scraper conveyor. Literature [17] has studied the key technology of hydraulic coupler and developed valve-controlled products, which can realize the soft start of high-power heavy-duty scraper conveyor. It is believed that the soft start technology can reduce the impact of starting current on the scraper conveyor. Document [18] analyzed the drive characteristics of the scraper conveyor coupling system, believed that CST can promote the stable operation of the scraper conveyor, studied the performance of the two-speed scraper conveyor motor drive system of the scraper conveyor, and proposed three schemes to improve the drive performance.

In order to finally achieve the purpose of online detection of scraper conveyor jamming and chain breakage, this paper proposes a method to determine the occurrence of scraper conveyor jamming and chain breakage by identifying the sudden change characteristics of driving scraper conveyor motor current, and simulates the scraper conveyor driving current characteristics by radial basis function neural network to improve the operating stability of scraper conveyor.

2 CURRENT SENSING SENSOR MODEL BASED ON RADIAL BASIS FUNCTION NEURAL NETWORK

2.1 Approximation control of RBF neural networks

The output of the sign function, time-varying parameters and external disturbances can cause large deviations and jitter in the fractional-order sliding mode control rate, which makes the observation of the magnetic chain and current based on the implementation less effective. In this paper, we use RBF neural network to approximate the optimal control rate in real time, so as to suppress the jitter caused by the sign function and parameter time-varying factors. The structure block diagram is shown in Figure 1.

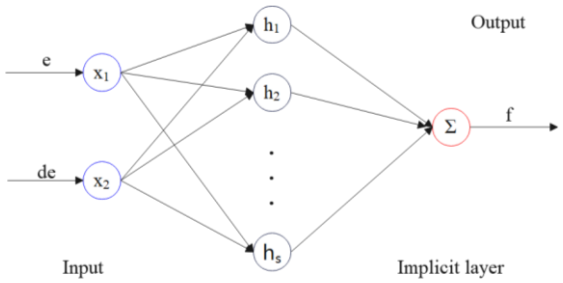

Figure 1 The structural diagram of the RBF neural network

Then, the optimal control rate should be[19]:

$$\rho^{*} = \rho - f \quad (1)$$

In the formula, f is the error of the control rate.

We use RBF neural network to approximate ρ^{*}, and its approximation algorithm is:

$$h_j = exp\left(\frac{\left\|x - c_{ij}\right\|^2}{2b_j^2}\right)$$
$$f = W^{*T}h(x) + \varepsilon \quad (2)$$

If the input of the neural network is defined as x=[x_1, x_2], its output is:

$$\hat{f}(x) = \hat{W}^T h(x) \quad (3)$$

We use formula (3) to approximate the optimal control rate and obtain a new control rate:

$$\begin{bmatrix}\rho_\alpha^* \\ \rho_\beta^*\end{bmatrix} = -\frac{k_2}{k_1}\begin{bmatrix}e_\alpha \\ e_\beta\end{bmatrix} + \frac{c_2}{c_1 k_1} D^{-\alpha+1}\begin{bmatrix}e_\alpha \\ e_\beta\end{bmatrix} + \frac{\mu_0}{c_1 k_1}\begin{bmatrix}sign(s_\alpha) \\ \sin g(s_\beta)\end{bmatrix} - \hat{f}(x) \quad (4)$$

By combining the obtained optimal control rate formula (4) and formula (1), we get:

$$\begin{bmatrix}\rho_\alpha \\ \rho_\beta\end{bmatrix} = -\frac{k_2}{k_1}\begin{bmatrix}e_\alpha \\ e_\beta\end{bmatrix} + \frac{c_2}{c_1 k_1} D^{-\alpha+1}\begin{bmatrix}e_\alpha \\ e_\beta\end{bmatrix} + \frac{\mu_0}{c_1 k_1}\begin{bmatrix}sign(s_\alpha) \\ \sin g(s_\beta)\end{bmatrix} + \left(f - \hat{f}(x)\right)$$
$$= -\frac{k_2}{k_1}\begin{bmatrix}e_\alpha \\ e_\beta\end{bmatrix} + \frac{c_2}{c_1 k_1} D^{-\alpha+1}\begin{bmatrix}e_\alpha \\ e_\beta\end{bmatrix} + \frac{\mu_0}{c_1 k_1}\begin{bmatrix}sign(s_\alpha) \\ \sin g(s_\beta)\end{bmatrix} + \tilde{f} \quad (5)$$

In the formula,

$$\tilde{f} = f - \hat{f}(x) = W^{*T}h(x) + \varepsilon - \tilde{W}^T h(x) + \varepsilon \quad (6)$$

and we define $\tilde{W} = W^{*T} - \hat{W}^T$.

Substituting formula (5) into the above formula, we can get:

$$\dot{s} = c_1 k_1 \begin{bmatrix}M \\ N\end{bmatrix} - \mu_0 \begin{bmatrix}sign(s_\alpha) \\ \sin g(s_\beta)\end{bmatrix} + c_1 k_1 \tilde{W}^T h - c_1 k_1 \varepsilon \quad (7)$$

In order to obtain the stable ideal approximation weight $\hat{W}$, the following Lyapunov function is selected:

$$L_2 = \frac{1}{2}s^2 + \frac{1}{2}\gamma \tilde{W}^T \tilde{W} \quad (8)$$

In the formula, γ >0.

By deriving the Lyapunov function L_2 and substituting formula (7) into the above formula, we get:

$$\dot{L}_2 = s\dot{s} + \gamma \tilde{W}^T \dot{\tilde{W}}$$
$$= c_1 k_1 \begin{bmatrix}M \\ N\end{bmatrix} - \mu_0 |s| + c_1 k_1 \tilde{W}^T h - c_1 k_1 \varepsilon s + \gamma \tilde{W}^T \dot{\tilde{W}} \quad (9)$$
$$= \left(c_1 k_1 \begin{bmatrix}M \\ N\end{bmatrix} - \mu_0 |s|\right) + \tilde{W}^T \left(c_1 k_1 s h + \gamma \dot{\tilde{W}}\right)$$

According to the result obtained in formula (9), the adaptive rate of the following formula is selected[20]:

$$\dot{\hat{W}} = -\frac{1}{\gamma} c_1 k_1 s h \tag{10}$$

$\dot{L}_2 < 0$ can be obtained by substituting formula (10) into formula (9), which shows that this adaptive law can make the system stable and achieve good approximation effect.

Therefore, by substituting the optimal control rate obtained by RBF neural network approximation into the formula, the optimal observed current can be obtained, and then the observed value of rotor flux linkage can be obtained by integrating it. The relationship is as follows:

$$\begin{bmatrix} \dot{\hat{i}}_{s\alpha} \\ \dot{\hat{i}}_{s\beta} \end{bmatrix} = k_1 \begin{bmatrix} \rho_\alpha^* \\ \rho_\beta^* \end{bmatrix} - k_2 \begin{bmatrix} \hat{i}_{s\alpha} \\ \hat{i}_{s\beta} \end{bmatrix} + k_3 \begin{bmatrix} \mu_{s\alpha} \\ \mu_{s\beta} \end{bmatrix}$$
$$\begin{bmatrix} \dot{\psi}_{r\alpha} \\ \dot{\psi}_{r\beta} \end{bmatrix} = -\begin{bmatrix} \rho_\alpha^* \\ \rho_\beta^* \end{bmatrix} \tag{11}$$

Finally, the observed current and flux values are substituted into the speed formula in the formula, and the final motor speed of scraper conveyor is obtained:

$$\dot{\omega}_r = \frac{n_p^2 L_m}{J L_r} \left(\hat{\psi}_{r\alpha} \hat{i}_{s\beta} - \hat{\psi}_{r\beta} \hat{i}_{s\alpha} \right) - \frac{n_p T_L}{J} \tag{12}$$

2.2 Power down-tolerant control of motor sensor power down of bearingless asynchronous scraper conveyor

Extended observer, also known as state reconstructor, is a control system that dynamically realizes the progressive estimation of the corresponding state variables according to the operating variables of the original system. We assume that there is a controlled object:

$$\dot{x} = f\left(x, v(t)\right) + ku(t) \tag{13}$$

When $a(t) = f\left(x, v(t)\right)$, it can be extended to a first-order state, and together with formula (13) to form a second-order system:

$$\begin{cases} \dot{x} = a(t) + ku(t) \\ \dot{a}(t) = b(t) \end{cases} \tag{14}$$

Therefore, formula (14) can be constructed, and the extended observer is:

$$\begin{cases} \dot{\hat{x}} = \hat{a}(t) + ku(t) + g_1\left(\hat{x} - x\right) \\ \dot{\hat{a}}(t) = g_2\left(\hat{x} - x\right) \end{cases} \tag{15}$$

The feedback function shown in the following formula is chosen:

$$g(x) = \begin{cases} c|x|^\eta \operatorname{sgn}(x), |x| > \delta \\ \dfrac{cx}{\delta^{1-\eta}}, |x| \le \delta \end{cases} \tag{16}$$

Based on the study of BL-IM mathematical model, with the current observation error as the system input and the rotor magnetic chain as the unknown term, the second-order expansion observer of the scraper conveyor motor

speed can be constructed as follows:

$$\begin{cases} \dot{i}_{s\alpha} = -k_2\hat{i}^*_{s\alpha} + k_3 u_{s\alpha} - k_1 a(t) + g_1\left(i_{s\alpha} - \hat{i}^*_{s\alpha}\right) \\ a(t) = g_2\left(i_{s\alpha} - \hat{i}^*_{s\alpha}\right) \\ \dot{i}_{s\beta} = -k_2\hat{i}^*_{s\beta} + k_3 u_{s\beta} - k_1 b(t) + g_1\left(i_{s\beta} - \hat{i}^*_{s\beta}\right) \\ b(t) = g_2\left(i_{s\beta} - \hat{i}^*_{s\beta}\right) \end{cases} \tag{17}$$

The input current and the uncertainty terms a(t) and b(t) can be well approximated by adjusting the three parameters c, η and δ in the feedback function, and the uncertainty terms can be integrated to obtain the estimated magnetic chain value:

$$\begin{cases} \hat{\psi}^*_{r\alpha} = \int_0^t a(t)\,dt \\ \hat{\psi}^*_{r\beta} = \int_0^t b(t)\,dt \end{cases} \tag{18}$$

Substituting the observed magnetic chain and current into formula (1), the formula for the derivative of the rotational speed can be obtained as shown in the following formula:

$$\dot{\omega}_r = \frac{n_p^2 L_m}{J L_r}\left(\hat{i}_{s\beta}\hat{\psi}_{r\alpha} - \hat{i}_{s\alpha}\hat{\psi}_{r\beta}\right) - \frac{n_p T_L}{J} \tag{19}$$

By integrating formula (19), the following observed velocities are obtained:

$$\hat{\omega}_r = \int_0^t \dot{\omega}_r dt \tag{20}$$

When the scraper conveyor motor is running normally, the observed rotational speed obtained by the designed expansion observer is close to the rotational speed observed by the sensor, and the error between the two is small at this time.

The simulation is built based on the designed expansion observer to obtain the speed error value of the expansion observer and the sensor during the power down-free operation of the scraper conveyor motor. We set the speed to 3000r/min and set the speed of the scraper conveyor motor to 4000r/min at 0.15s and add 2N-m load at 0.2s to obtain the error curve as shown in Figure 2. It is not difficult to find from the figure that in the no-load starting stage of the scraper conveyor motor, the speed error reaches a maximum value of about 130r/min. Therefore, on the basis of leaving a certain deviation, the judgment threshold of rotational speed is set at 150r/min.

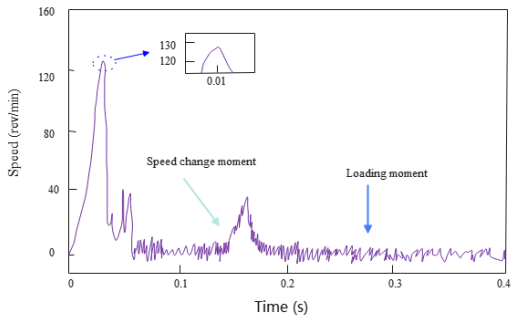

Figure 2 Speed error curve of expansion observer and sensor

The error diagnosis of the speed sensor is performed according to the designed threshold, and when it is in error,

if the speed sensor speed is directly used as the output, the speed closed loop will be broken, thus making it impossible to quickly tolerate the error after a speed sensor failure. Therefore, in this paper, the sensor speed and the observed speed are proportionally added to obtain the feedback speed after fusing the data, as shown in formula (21), and it is used as the feedback of the closed loop of the speed, so as to solve the problem of the closed loop breaking when the power down occurs.

$$\hat{\omega}_r^* = \xi_1 \omega_r + \xi_2 \hat{\omega}_r \tag{21}$$

Choosing the appropriate fusion coefficient will accelerate the convergence speed during acceleration and deceleration. $\xi_1 = 0.8$ and $\xi_2 = 0.2$ are selected through a large number of simulations, thus obtaining the power down-tolerant control flow chart of speed sensor as shown in Figure 3.

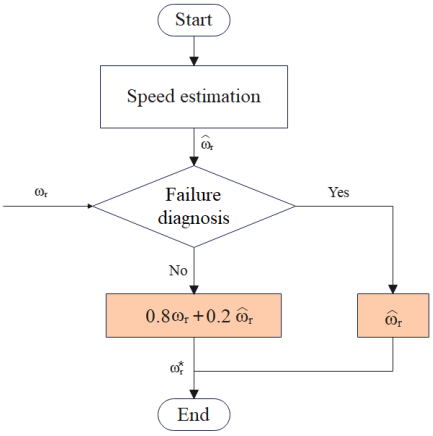

Figure 3 Flowchart of sensor power down-tolerant control

For the equation of state of BL-IM in the stationary coordinate system, we set the output variable as:

$$Y = \begin{bmatrix} \psi_{r\beta} & i_{s\alpha} & i_{s\beta} \end{bmatrix}^T \tag{22}$$

Among them, the state variable is:

$$X = \begin{bmatrix} \psi_{r\alpha} & \psi_{r\beta} & i_{s\alpha} & i_{s\beta} \end{bmatrix}^T \tag{23}$$

The input variable is:

$$U = \begin{bmatrix} \omega & T_L & u_{s\alpha} & u_{s\beta} \end{bmatrix}^T \tag{24}$$

By inputting known input variables into the state equation, the set output variables are obtained, allowing the observation of current in the stationary coordinate system.

When the sensor is operating normally, the error $g_1\left(i_s - \hat{i}_s^*\right)$ of the current and the derivative $g_2\left(i_s - \hat{i}_s^*\right)$ of the uncertain magnetic chain containing both the magnetic chain and the total disturbance in the ideal state can be obtained according to formula (17).

The derivative of the observed magnetic chain is expressed by the formula:

$$\begin{cases} g_2\left(i_{s\alpha} - \hat{i}_{s\alpha}^*\right) = \dot{\psi}_{r\alpha} + f_\alpha \\ g_2\left(i_{s\beta} - \hat{i}_{s\beta}^*\right) = \dot{\psi}_{r\beta} + f_\beta \end{cases} \tag{25}$$

Therefore, the error of the observed flux derivative can be obtained as follows:

$$f_\alpha = g_2\left(i_{s\alpha} - \hat{i}^*_{s\alpha}\right) - \hat{\dot{\psi}}_{r\alpha} = g_2\left(i_{s\alpha} - \hat{i}^*_{s\alpha}\right) + \frac{1}{T_r}\hat{\psi}^*_{r\alpha} - \frac{L_m}{T_r}\hat{i}^*_{s\alpha} + \omega_r\hat{\dot{\psi}}_{r\beta} \tag{26}$$

$$f_\beta = g_2\left(i_{s\beta} - \hat{i}^*_{s\beta}\right) - \hat{\dot{\psi}}_{r\beta} = g_2\left(i_{s\beta} - \hat{i}^*_{s\beta}\right) + \frac{1}{T_r}\hat{\psi}^*_{r\beta} - \frac{L_m}{T_r}\hat{i}^*_{s\beta} + \omega_r\hat{\dot{\psi}}_{r\alpha} \tag{27}$$

Using current error and flux derivative error for two-phase compensation, the state equation of new scraper conveyor motor for current observation can be obtained as follows:

$$\begin{cases} \hat{\dot{i}}_{s\alpha} = -k_1\hat{\dot{\psi}}_{r\alpha} - k_2\hat{i}_{s\alpha} + k_3 u_{s\alpha} + g_1\left(i_{s\alpha} - \hat{i}^*_{s\alpha}\right) \\ \hat{\dot{i}}_{s\beta} = -k_1\hat{\dot{\psi}}_{r\beta} - k_2\hat{i}_{s\beta} + k_3 u_{s\beta} + g_1\left(i_{s\beta} - \hat{i}^*_{s\beta}\right) \\ \hat{\dot{\psi}}_{r\alpha} = -\frac{1}{T_r}\hat{\psi}_{r\alpha} - \omega_r\hat{\dot{\psi}}_{r\beta} + \frac{L_m}{T_r}\hat{i}_{s\alpha} + f_\alpha \\ \hat{\dot{\psi}}_{r\beta} = -\frac{1}{T_r}\hat{\psi}_{r\beta} - \omega_r\hat{\dot{\psi}}_{r\alpha} + \frac{L_m}{T_r}\hat{i}_{s\beta} + f_\beta \end{cases} \tag{28}$$

Since the current observation equation of state is based on the stationary coordinate system, the sensor and the feedback current are three-phase currents. Therefore, it is necessary to convert the currents in the stationary coordinate system and the currents in the three-phase coordinate system to each other. Usually, there are two conversion methods, and the coordinate system position relationship is shown in Figure 4.

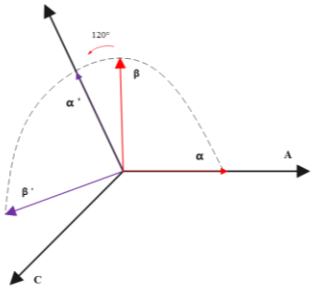

Figure 4 Position relationship between stationary and three-phase coordinate system

When the axis of phase α is in the same direction as the axis of A-phase, the relationship between $i_{\alpha\beta}$ and i_{ABC} can be obtained as:

$$\begin{bmatrix} i_\alpha \\ i_\beta \end{bmatrix} = \begin{bmatrix} \sqrt{\frac{3}{2}} & 0 \\ \frac{1}{\sqrt{2}} & \sqrt{2} \end{bmatrix} \begin{bmatrix} i_A \\ i_B \end{bmatrix} \tag{29}$$

$$\begin{bmatrix} i_{A1} \\ i_{B1} \\ i_{C1} \end{bmatrix} = \begin{bmatrix} \sqrt{\frac{3}{2}} & 0 \\ -\frac{1}{\sqrt{6}} & \frac{1}{\sqrt{2}} \\ -\frac{1}{\sqrt{6}} & -\frac{1}{\sqrt{2}} \end{bmatrix} \quad (30)$$

When the α-phase axis is in the same direction as the B -phase axis, the new relationship between $i'_{\alpha\beta}$ and i'_{ABC} can be obtained as:

$$\begin{bmatrix} i'_{\alpha} \\ i'_{\beta} \end{bmatrix} = \begin{bmatrix} 0 & \sqrt{\frac{3}{2}} \\ -\sqrt{2} & -\frac{1}{\sqrt{2}} \end{bmatrix} \begin{bmatrix} i_A \\ i_B \end{bmatrix} \quad (31)$$

$$\begin{bmatrix} i_{A2} \\ i_{B2} \\ i_{C2} \end{bmatrix} = \begin{bmatrix} -\frac{1}{\sqrt{6}} & -\frac{1}{\sqrt{2}} \\ \sqrt{\frac{2}{3}} & 0 \\ -\frac{1}{\sqrt{6}} & \frac{1}{\sqrt{2}} \end{bmatrix} \quad (32)$$

Under normal conditions, the first coordinate transformation is chosen as the conversion between currents in this paper. The feedback three-phase currents are converted to the stationary coordinate system to obtain i_{sab} , and then the observed currents in the stationary coordinate system are obtained by using formula (28), and finally converted to the three-phase coordinate system to obtain the observed three-phase currents.

When the sensor is power downy, the feedback three-phase current is not perfect, and the current in the stationary coordinate system cannot be solved directly by formula (28) at this time. Therefore, when the power down occurs in the A-phase current sensor, the single-phase compensation can be performed according to the correct i, and then the compensated three-phase current i_{ABC2} can be obtained using formula (32). similarly, when the power down occurs in the B-phase current sensor, the compensated three-phase current i_{ABC1} can be obtained using formula (30). At this point, the equation of state of the scraper conveyor motor used for current observation after single-phase compensation is:

$$\begin{cases} \dot{i}_{s\alpha} = -k_1\dot{\psi}_{r\alpha} - k_2\hat{i}_{s\alpha} + k_3 u_{s\alpha} + g_1\left(i_{s\alpha} - \hat{i}^*_{s\alpha}\right) \\ \dot{i}_{s\beta} = -k_1\dot{\psi}_{r\beta} - k_2\hat{i}_{s\beta} + k_3 u_{s\beta} \\ \dot{\psi}_{r\alpha} = -\frac{1}{T_r}\hat{\psi}_{r\alpha} - \omega_r\hat{\psi}_{r\beta} + \frac{L_m}{T_r}\hat{i}_{s\alpha} + f_{\alpha} \\ \dot{\psi}_{r\beta} = -\frac{1}{T_r}\hat{\psi}_{r\beta} - \omega_r\hat{\psi}_{r\alpha} + \frac{L_m}{T_r}\hat{i}_{s\beta} \end{cases} \quad (33)$$

When solving for f_{α} , the ideal magnetic chain $\dot{\psi}_{r\beta}$ in formula (26) is affected by the i_{β} -power down cannot

be measured by the expansion observer and can be replaced by using the equation of state observations that do not differ much from it.

When a two-phase power down occurs in the current sensor, the compensation of both the current and the magnetic chain fails, and the current can only be solved using the ideal state equation.

The current error diagrams for full compensation when the current sensor is not power downy and for single-phase compensation when a single-phase power down occurs are obtained by simulation, as shown in Figure 5. We set the current sensor power down diagnosis thresholds for A-phase and B-phase to 0.3A and 0.35A, respectively, when the current sensor is not power downy. When the current sensor is single-phase power downy, the power down diagnosis threshold of the current sensor is 0.3A for both A-phase and B-phase.

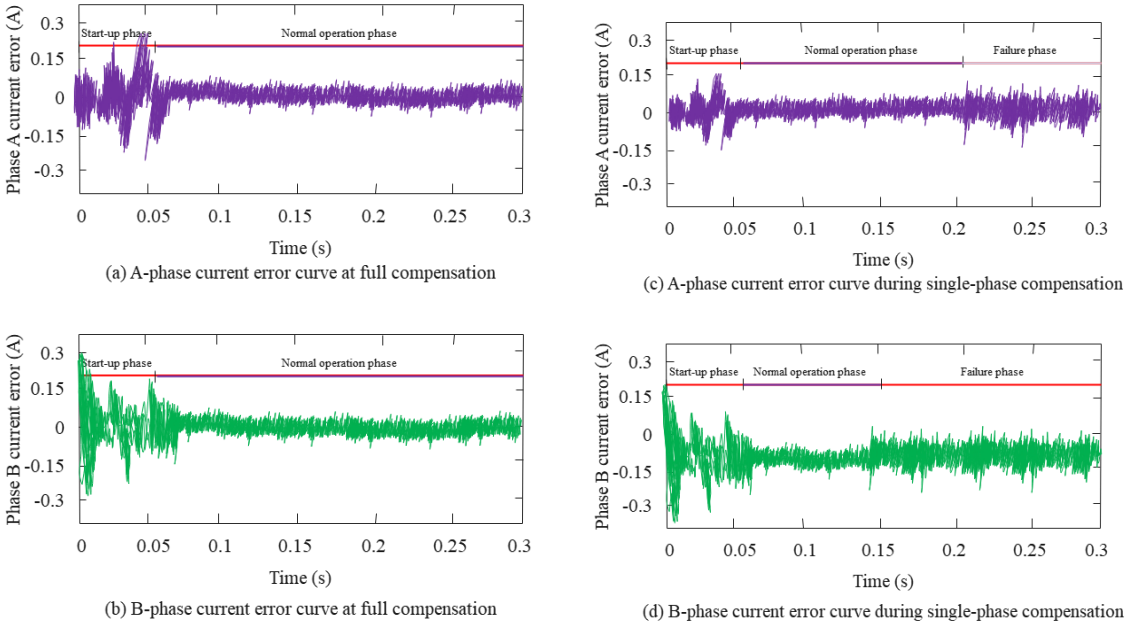

(a) A-phase current error curve at full compensation

(c) A-phase current error curve during single-phase compensation

(b) B-phase current error curve at full compensation

(d) B-phase current error curve during single-phase compensation

Figure 5 Observation error curve of current sensor

When using single-phase power downs, we perform power down tolerance based on the power down phase currents $\hat{i}_{B1}$ and $\hat{i}_{A1}$ obtained from the equation of state of the scraper conveyor motor after single-phase compensation and the power down phase currents $\hat{i}_A$ and $\hat{i}_B$ obtained from the ideal state equation at full power down.

3 SIMULATION OF DRIVING CURRENT CHARACTERISTICS OF COAL MINE SCRAPER CONVEYOR

This paper takes coal mine scraper conveyor as the research object, and carries out the technical base research with the goal of finally realizing online power down targeting of scraper conveyor and finally realizing power down detection. The scraper conveyor's broken chain scene and the scraper fracture diagram caused by the broken chain are shown in Figure 6.

(a) Scraper conveyor's broken chain scene (b) Scraper fracture caused by broken chain

Figure 6 Scraper conveyor's broken chain scene and the scraper fracture diagram caused by the broken chain

The scraper condition monitoring system is composed of the permanent magnet variable frequency integrated machine condition monitoring system and the scraper chain condition monitoring system, and its overall scheme is shown in Figure 7.

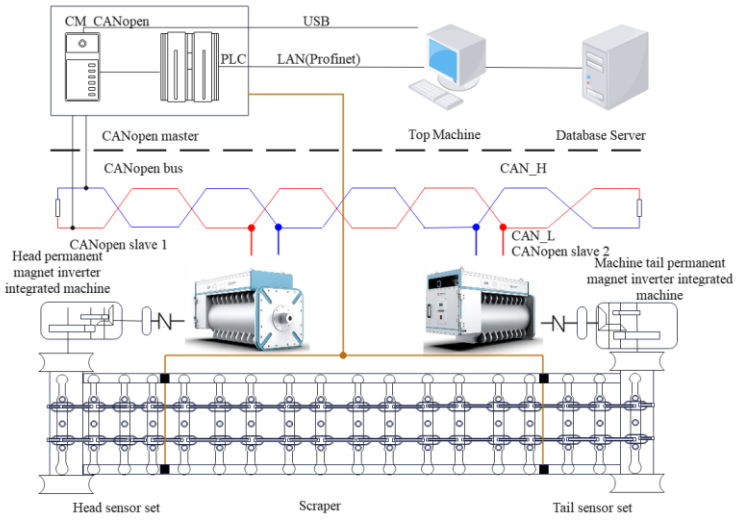

Figure 7 Overall scheme of the condition monitoring system

In order to verify the effectiveness of the speed and current power down-tolerant control system, a simulation model is built using MATLAB/Simulink and a simulation study is carried out.

Since the scraper conveyor motor is in no-load and load conditions most of the time in daily applications, the simulation was carried out for both cases to obtain the speed simulation curves in Figure 8. Figure 8(a) and Figure 8(b) represent the speed curves under power down-tolerant control when the scraper conveyor motor is running at no load and at load, respectively. Figure 8(c) shows the rotor position curve under power down-tolerant control during load operation.

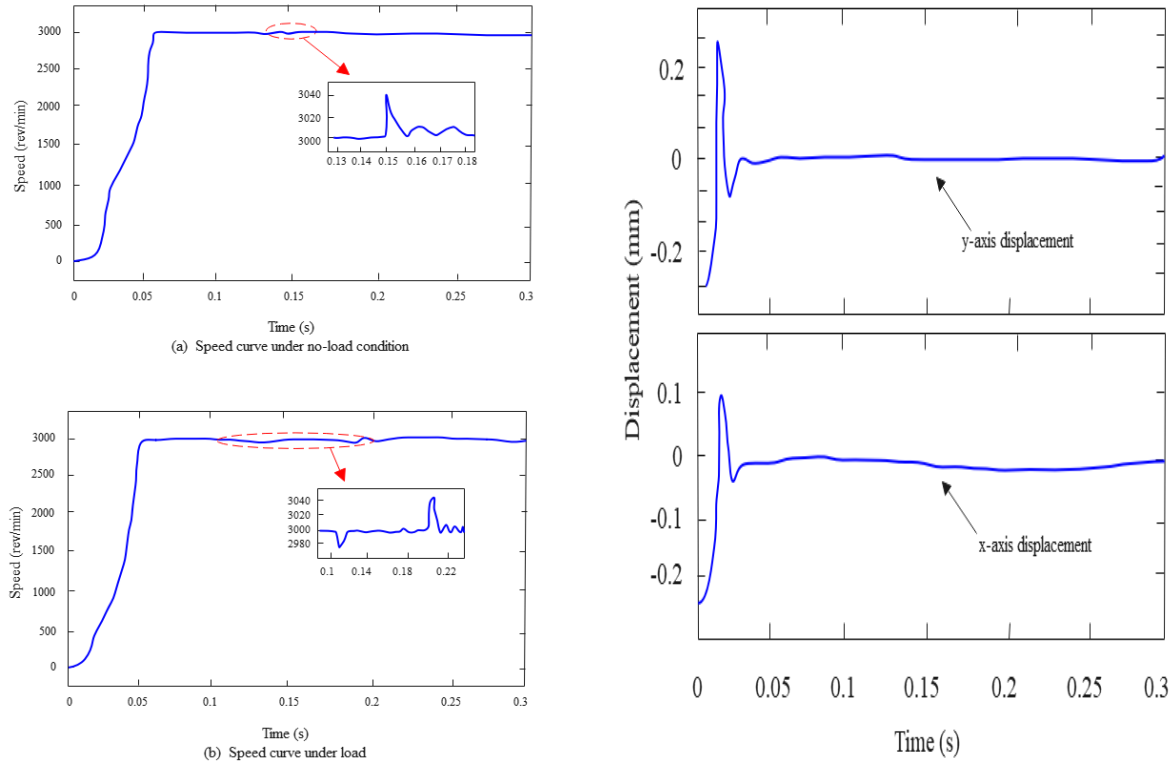

Figure 8 Simulation diagram of speed sensor failure

In this paper, the simulation was verified for sensor power downs in three cases, A-phase, B-phase and A- and B-phase, and the simulation results shown in Figure 9, Figure 10 and Figure 11 are obtained.

Figure 9 shows the simulation results of the A-phase current sensor when the power down occurs at 0.15s, and then switch to the second current coordinate transformation method. Figure 9(a) shows the error curve between the observed value of A-phase current with and without compensation and the actual current value. Figure 9(b) shows the observed values of the A-phase current before and after the power down, which is affected by the power down after 0.15s with some disturbance, but the overall effect is not significant. Figure 9(c) shows the speed curve of the scraper conveyor motor. The scraper conveyor motor runs normally when there is no power down, but after the power down, there is an error fluctuation of 1.5r/min due to the observation current error.

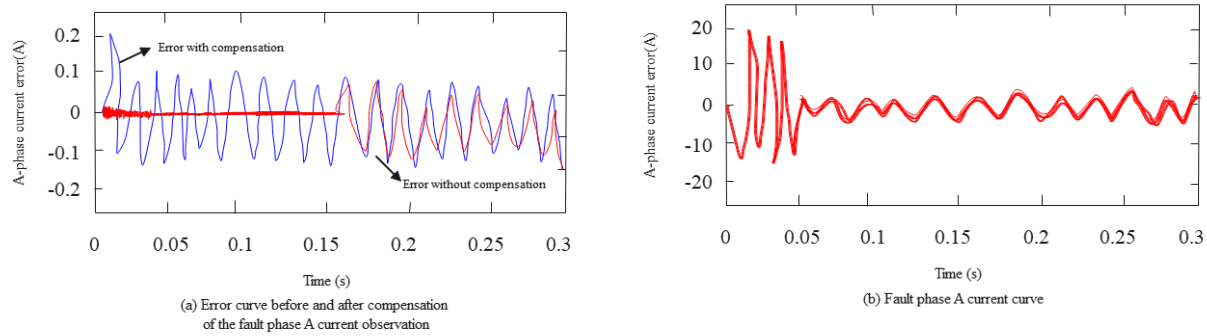

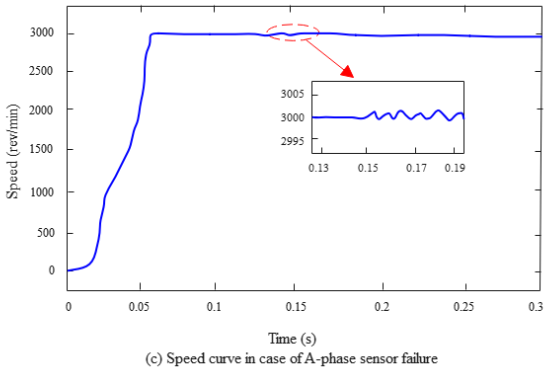

Figure 9 Simulation diagram when the A-phase current sensor fails

Figure 10 shows the simulation results of a power down in the B-phase current sensor at 0.2s. In this case, the first current coordinate change method is chosen. Figure 10 (a) and 10 (B) are the error curves between the observed value of B-phase current and the actual current value with and without compensation, and the observed value of B-phase current, respectively. Figure 10 (c) shows the speed curve of the scraper conveyor motor. Before the power down, the scraper conveyor motor runs normally, but after the power down, the speed decreases first, and then recovers to fluctuate within the error of 2r/min.

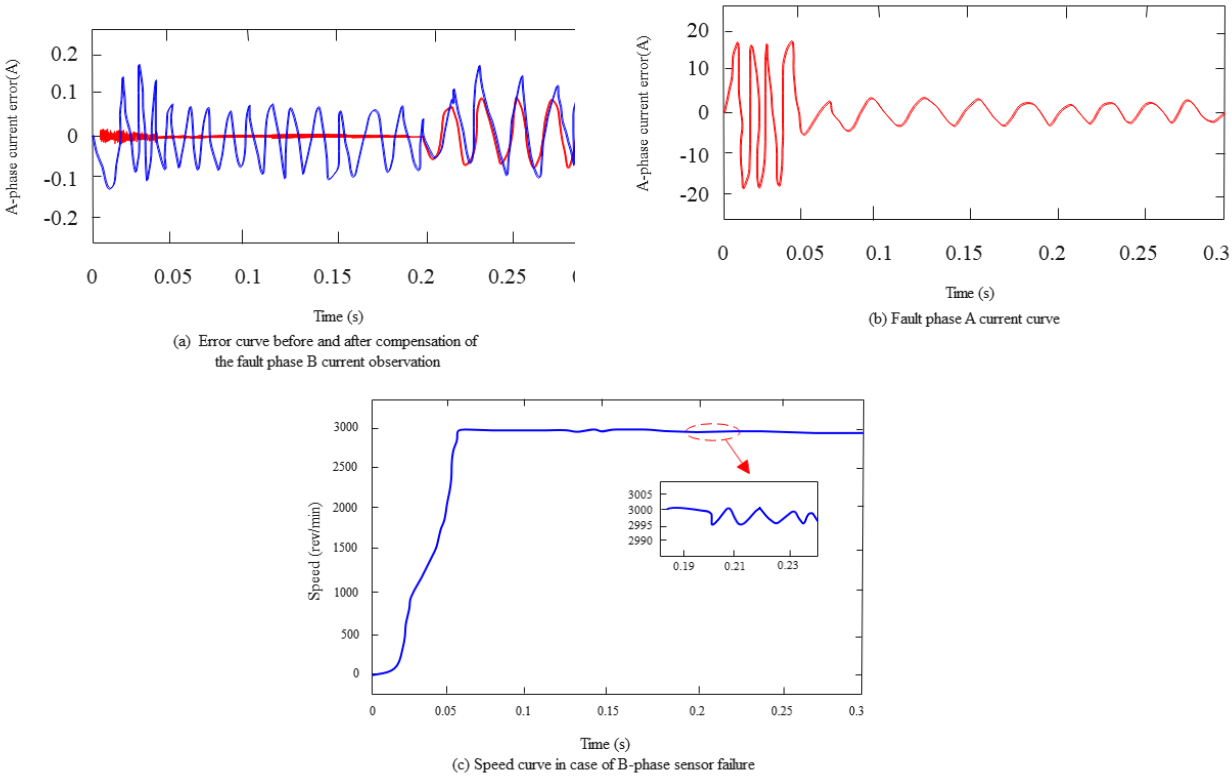

Figure 10 Simulation diagram when the A-phase current sensor fails

Figure 11 shows the simulation diagram of BL-IM in 0.15 s and 0.2 s when the A-phase and B-phase current sensors fail respectively. Figure 11(a) and Figure 11(b) show the observed values of A-phase and B-phase currents, respectively. The overall waveform is not much different from that of the single-phase power down, but the burr increases due to the larger error. Figure 11(C) indicates the speed curve of the scraper conveyor motor.

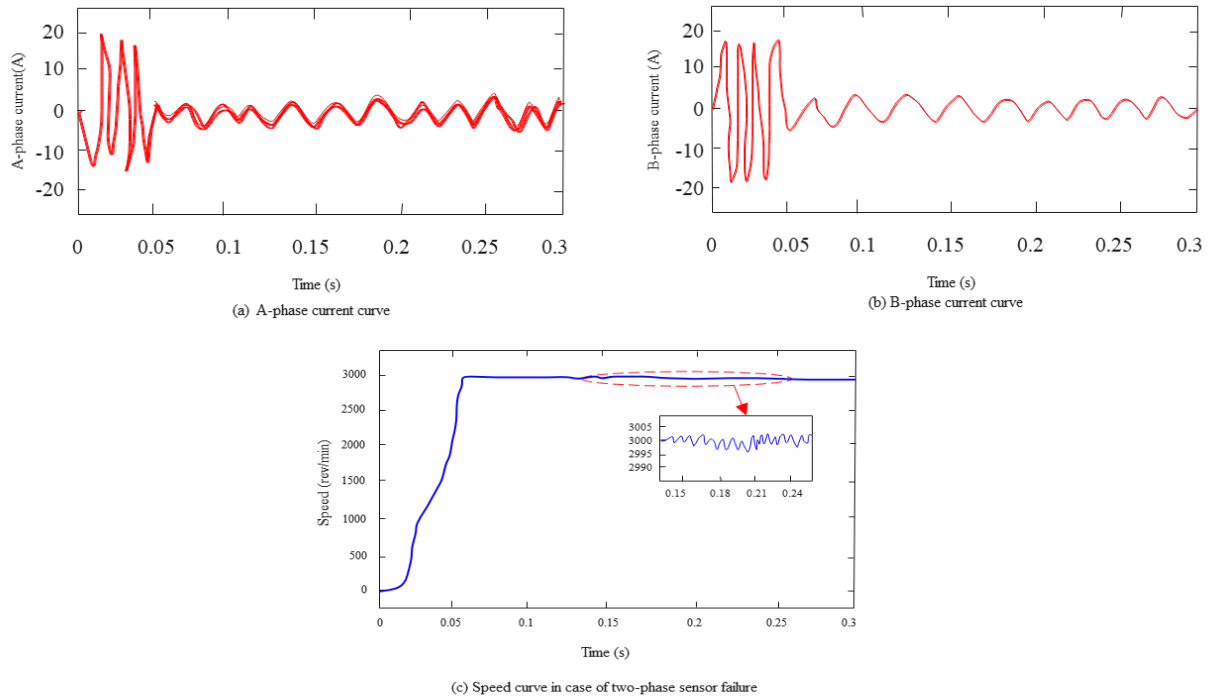

Figure 11 Simulation diagram when the two-phase current sensor fails

The above simulation results verify that the simulation method of scraper conveyor drive current characteristics based on radial basis function neural network proposed in this paper can effectively improve the analysis effect of scraper conveyor drive current characteristics, which has some practical significance for the power down detection of scraper conveyor.

4 CONCLUSION

In order to adapt to the development direction of scraper conveyor, this paper adopts multiple scraper conveyor motors for load drive, which has gradually developed into the main driving mode of scraper conveyor. In this paper, a power down-tolerant control strategy based on radial basis function neural network for driving current characteristic sensor of scraper conveyor is proposed. The diagnosis and power down-tolerant control of the speed sensor are realized by using the expansion principle and data fusion method, and then the diagnosis and power down-tolerant control of the current sensor are realized by the compensation state equation of the expansion observer. On this basis, the power down tolerance of speed sensor under no-load and load conditions, and the power down tolerance of single-phase current and two-phase current sensors are simulated. The results show that the proposed control strategy can not only realize power down diagnosis and power down-tolerant control of speed and current sensors, but also avoid the influence of long-time sensor power down on rotor suspension, which shows that the power down-tolerant control method designed in this paper is effective.

ACKNOWLEDGE:

2023 Inner Mongolia Natural Science Foundation Project "Research on Fault Diagnosis Method of Low-speed Semi-direct Drive Wind Turbine Based on Deep Transfer Learning" (No. 2023LHMS05043);

National Natural Science Foundation of China (NSFC) "Research on the Fault Evolution Mechanism and Condition Monitoring Theory of Main Bearing of Intermittent Low-speed Variable-load Direct Drive Fan" (No. 51965052);

2022 Basic Scientific Research Funds for Universities Directly under the Autonomous Region;

In 2022, the scientific research and innovation team of Baotou Vocational and Technical College was funded for the construction project of "Independent Innovation Research on Enterprise Flexible Intelligent Production Line".

REFERENCES

[1] Li, D., & Wang, S. (2021). Characteristics of new permanent magnetic eddy current drive system of the scraper conveyor. The Journal of Engineering, 2021(10), 552-558.

[2] Zhao, S., Wang, P., & Li, S. (2020). Study on the fault diagnosis method of scraper conveyor gear under time-varying load condition. Applied Sciences, 10(15), 5053-5062.

[3] Xia, R., Li, B., Wang, X., Yang, Z., & Liu, L. (2019). Screening the Main Factors Affecting the Wear of the Scraper Conveyor Chute Using the Plackett–Burman Method. Mathematical Problems in Engineering, 2019(3), 1-11.

[4] Liu, T., Tan, C., Wang, Z., Xu, J., Man, Y., & Wang, T. (2019). Horizontal bending angle optimization method for scraper conveyor based on improved bat algorithm. Algorithms, 12(4), 84-93.

[5] Florea, V. A., Pasculescu, D., & Pasculescu, V. M. (2021). Reliability and maintainability of scraper conveyor used in coal mining in the Jiu Valley. Mining of Mineral Deposits, 15(3), 16-21.

[6] Zhang, X., Li, W., Zhu, Z., & Jiang, F. (2020). Fault detection for scraper chain using an observer-based tension distribution estimation algorithm. Current Science, 118(11), 1792.

[7] Dai, K., Zhu, Z., Tang, Y., Shen, G., Li, X., & Sa, Y. (2021). Position synchronization tracking of multi-axis drive system using hierarchical sliding mode control. Journal of the Brazilian Society of Mechanical Sciences and Engineering, 43(3), 1-16.

[8] Hao, J., Song, Y., Zhang, P., Liu, H., Jia, S., Zheng, Y., & Zhang, X. (2022). Failure analysis of scraper conveyor based on fault tree and optimal design of new scraper with polyurethane material. Journal of Materials Research and Technology, 18(5), 4533-4548.

[9] Wang, Z., Li, B., Liang, C., Wang, X., & Li, J. (2021). Response Analysis of a Scraper Conveyor under Chain Faults Based on MBD-DEM-FEM. Strojniski Vestnik-Journal of Mechanical Engineering, 67(10), 501-516.

[10] Zhang, Q., Zhang, R. X., & Tian, Y. (2020). Scraper conveyor structure improvement and performance comparative analysis. Strength of Materials, 52(4), 683-690.

[11] Wang, Y., Guo, W., Zhao, S., Xue, B., Zhang, W., & Xing, Z. (2022). A Big Coal Block Alarm Detection Method for Scraper Conveyor Based on YOLO-BS. Sensors, 22(23), 9052-9566.

[12] Xia, R., Wang, X., Li, B., Wei, X., & Yang, Z. (2019). The prediction of wear on a scraper conveyor chute affected by different factors based on the discrete element method. Proceedings of the Institution of Mechanical Engineers, Part C: Journal of Mechanical Engineering Science, 233(17), 6229-6239.

[13] Hua, Y., Zhu, Z., Zhou, G., & Shen, G. (2021). Chain State Monitoring for a Heavy Scraper Conveyor Using UWB-Based Extended Kalman Filter Technique With Range Constraint Selection Method. IEEE Transactions on Instrumentation and Measurement, 71(6), 1-9.

[14] Xiao, Y., Li, Y., & Chu, C. (2021). Performance Analysis of Vibration Sensors for Closed-Loop Feedback Health Monitoring of Mechanical Equipment. Journal of Sensors, 2021(2), 1-12.

[15] Келисбеков, А. К., Данияров, Н. А., Ахметбекова, А. М., & Оразбаев, К. Н. (2021). CONTROL OF STARTING MODES OF AN APRON CONVEYOR MULTI-MOTOR ELECTRIC DRIVE. Eurasian Physical Technical Journal, 18(4 (38)), 74-81.

[16] Ma, H., Wang, X., Li, B., Liu, Z., Bi, W., & Wei, X. (2022). Study on the mechanical effect and wear behaviour of middle trough of a scraper conveyor based on DEM–MBD. Proceedings of the Institution of Mechanical Engineers, Part J: Journal of Engineering Tribology, 236(7), 1363-1374.

[17] Shuai, L., Zhencai, Z., Hao, L., & Gang, S. (2019). A system reliability-based design optimization for the scraper chain of scraper conveyors with dependent failure modes. Eksploatacja i Niezawodność, 21(3), 392-402.

[18] Lu, E., Li, W., Yang, X., & Liu, Y. (2019). Anti-disturbance speed control of low-speed high-torque PMSM based on second-order non-singular terminal sliding mode load observer. ISA transactions, 88(1), 142-152.

[19] Xing, Z., Zhao, S., Guo, W., Guo, X., & Wang, Y. (2021). Processing laser point cloud in fully mechanized mining face based on DGCNN. ISPRS International Journal of Geo-Information, 10(7), 482-491.

[20] Li, S., Zhu, Z., Lu, H., & Shen, G. (2021). Time-dependent reliability and optimal design of scraper chains based on fretting wear process. Engineering Computations, 38(10), 3673-3693.